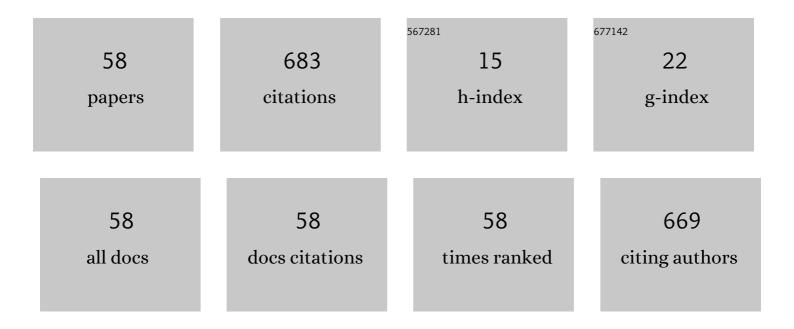
## Shuangmeng Zhai

List of Publications by Year in descending order

Source: https://exaly.com/author-pdf/241135/publications.pdf Version: 2024-02-01



#	Article	IF	CITATIONS
1	Pressure generation and investigation of the post-perovskite transformation in MgGeO3 by squeezing the Kawai-cell equipped with sintered diamond anvils. Earth and Planetary Science Letters, 2010, 293, 84-89.	4.4	43
2	Pâ€Vâ€T relations of MgSiO <sub>3</sub> perovskite determined by in situ Xâ€ray diffraction using a largeâ€volume highâ€pressure apparatus. Geophysical Research Letters, 2009, 36, .	4.0	39
3	Spin transition of ferric iron in the NAL phase: Implications for the seismic heterogeneities of subducted slabs in the lower mantle. Earth and Planetary Science Letters, 2016, 434, 91-100.	4.4	30
4	Tuite, γ a <sub>3</sub> ( <scp>PO</scp> <sub>4</sub> ) <sub>2</sub> , formed by chlorapatite decomposition in a shock vein of the Suizhou L6 chondrite. Meteoritics and Planetary Science, 2013, 48, 1515-1523.	1.6	29
5	<i>P</i> â€ <i>V</i> â€ <i>T</i> relations of wadsleyite determined by in situ Xâ€ray diffraction in a largeâ€volume highâ€pressure apparatus. Geophysical Research Letters, 2009, 36, .	4.0	27
6	Highâ€pressure Raman spectra of tuite, γ a <sub>3</sub> (PO <sub>4</sub> ) <sub>2</sub> . Journal of Raman Spectroscopy, 2010, 41, 1011-1013.	2.5	26
7	Thermal diffusivity and thermal conductivity of granitoids at 283–988 K and 0.3–1.5 GPa. American Mineralogist, 2019, 104, 1533-1545.	1.9	24
8	Equation of state of Â-tricalcium phosphate, Â-Ca3(PO4)2, to lower mantle pressures. American Mineralogist, 2009, 94, 1388-1391.	1.9	23
9	A comparison of the Ca3(PO4)2 and CaSiO3 systems, with a new structure refinement of tuite synthesized at 15 GPa and 1300 ÂC. American Mineralogist, 2013, 98, 1585-1592.	1.9	22
10	Compressibility of strontium orthophosphate Sr3(PO4)2 at high pressure. Physics and Chemistry of Minerals, 2011, 38, 357-361.	0.8	20
11	Effect of Water on the Thermal Properties of Olivine With Implications for Lunar Internal Temperature. Journal of Geophysical Research E: Planets, 2019, 124, 3469-3481.	3.6	19
12	Elasticity of singleâ€crystal superhydrous phase B at simultaneous high pressureâ€temperature conditions. Geophysical Research Letters, 2016, 43, 8458-8465.	4.0	18
13	Raman spectra and X-ray diffraction of tuite at various temperatures. Physics and Chemistry of Minerals, 2011, 38, 639-646.	0.8	17
14	Synthesis and photoluminescence properties of Eu3+-doped γ-Ca3(PO4)2. Materials Chemistry and Physics, 2012, 133, 324-327.	4.0	17
15	X-ray diffraction study of -Ca3(PO4)2 at high pressure. Solid State Communications, 2010, 150, 443-445.	1.9	15
16	Raman spectra of Sr3(PO4)2 and Ba3(PO4)2 orthophosphates at various temperatures. Vibrational Spectroscopy, 2014, 70, 6-11.	2.2	15
17	Pressure-dependent Raman spectra of β-Ca3(PO4)2 whitlockite. Physics and Chemistry of Minerals, 2015, 42, 303-308.	0.8	15
18	Electrical Resistivity of Iron Phosphides at Highâ€Pressure and Highâ€Temperature Conditions With Implications for Lunar Core's Thermal Conductivity. Journal of Geophysical Research: Solid Earth, 2019, 124, 5544-5556.	3.4	15

SHUANGMENG ZHAI

#	Article	IF	CITATIONS
19	Raman spectra of stronadelphite Sr5(PO4)3F at high pressures. Physics and Chemistry of Minerals, 2015, 42, 579-585.	0.8	14
20	Si-Al distribution in high-pressure CaAl4Si2O11 phase: A 29Si and 27Al NMR study. American Mineralogist, 2009, 94, 1739-1742.	1.9	13
21	High-pressure Raman spectroscopic studies on orthophosphates Ba3(PO4)2 and Sr3(PO4)2. Solid State Communications, 2011, 151, 276-279.	1.9	13
22	Single crystal growth, crystalline structure investigation and high-pressure behavior of impurity-free siderite (FeCO3). Physics and Chemistry of Minerals, 2018, 45, 831-842.	0.8	13
23	Raman spectra of sillimanite, andalusite, and kyanite at various temperatures. Physics and Chemistry of Minerals, 2020, 47, 1.	0.8	13
24	P-V-T relations of Â-Ca3(PO4)2 tuite determined by in situ X-ray diffraction in a large-volume high-pressure apparatus. American Mineralogist, 2013, 98, 1811-1816.	1.9	12
25	Thermodynamic investigation on β- and γ-Ca3(PO4)2 and the phase equilibria. Physics of the Earth and Planetary Interiors, 2014, 228, 144-149.	1.9	11
26	Compressibilities of MnFe2O4 polymorphs. Physics and Chemistry of Minerals, 2015, 42, 569-577.	0.8	11
27	High-pressure X-ray diffraction and Raman spectroscopy of CaFe2O4-type β-CaCr2O4. Physics and Chemistry of Minerals, 2016, 43, 307-314.	0.8	11
28	Phase boundary between perovskite and post-perovskite structures in MnGeO3 determined by in situ X-ray diffraction measurements using sintered diamond anvils. American Mineralogist, 2011, 96, 89-92.	1.9	10
29	Raman spectra and X-ray diffraction of merrillite at various temperatures. Vibrational Spectroscopy, 2020, 106, 103005.	2.2	10
30	Effect of temperature on the Raman spectra of Ca5(PO4)3F fluorapatite. European Journal of Mineralogy, 2018, 30, 951-956.	1.3	10
31	Synthesis and characterization of strontium–calcium phosphate γ-Ca3â^'xSrx(PO4)2 (0≤â‰⊉). Materials Chemistry and Physics, 2010, 120, 348-350.	4.0	9
32	The phase diagram of the Fe-P binary system at 3â€ <sup>−</sup> GPa and implications for phosphorus in the lunar core. Geochimica Et Cosmochimica Acta, 2019, 254, 54-66.	3.9	9
33	Phase boundary between ilmenite and perovskite structures in MnGeO3 determined by in situ X-ray diffraction measurements. Physics and Chemistry of Minerals, 2007, 34, 269-273.	0.8	8
34	Electrical Resistivity of Fe and Feâ€3 wt%P at 5ÂGPa With Implications for the Moon's Core Conductivity and Dynamo. Journal of Geophysical Research E: Planets, 2022, 127, .	3.6	8
35	Effects of pre-heated pyrophyllite gaskets on high-pressure generation in the Kawai-type multi-anvil experiments. High Pressure Research, 2008, 28, 265-271.	1.2	7
36	Elasticity of singleâ€crystal NAL phase at high pressure: A potential source of the seismic anisotropy in the lower mantle. Journal of Geophysical Research: Solid Earth, 2016, 121, 5696-5707.	3.4	7

SHUANGMENG ZHAI

#	Article	IF	CITATIONS
37	Spin transition of ferric iron in the calciumâ€ferrite type aluminous phase. Journal of Geophysical Research: Solid Earth, 2017, 122, 5935-5944.	3.4	7
38	Raman spectroscopic study of stronadelphite Sr5(PO4)3F at various temperatures. Vibrational Spectroscopy, 2018, 98, 123-127.	2.2	7
39	The structure-Raman spectra relationships of Mg3(PO4)2 polymorphs: A comprehensive experimental and DFT study. Spectrochimica Acta - Part A: Molecular and Biomolecular Spectroscopy, 2021, 245, 118906.	3.9	7
40	Compressibility of pyrochlore-type MgZrSi2O7determined byin situX-ray diffraction in a large-volume high pressure apparatus. High Pressure Research, 2013, 33, 1-7.	1.2	6
41	Trace element composition in tuite decomposed from natural apatite in high-pressure and high-temperature experiments. Science China Earth Sciences, 2014, 57, 2922-2927.	5.2	6
42	Photoluminescence properties of $\hat{1}^3$ -Ca3(PO4)2:Sm3+ prepared under high-pressure and high-temperature conditions. Optical Materials, 2015, 45, 219-223.	3.6	5
43	Temperature-induced phase transition of Ca2AlSiO5.5: Raman spectroscopic study. Vibrational Spectroscopy, 2019, 103, 102935.	2.2	5
44	Thermal diffusivity and thermal conductivity of alkali feldspar at 0.8–3 GPa and 300–873 K. Contributions To Mineralogy and Petrology, 2021, 176, 1.	3.1	5
45	Raman spectroscopic study of MnAl2O4 galaxite at various pressures and temperatures. Physics and Chemistry of Minerals, 2017, 44, 163-170.	0.8	4
46	High-pressure in-situ X-ray diffraction and Raman spectroscopy of Ca <sub>2</sub> AlFeO <sub>5</sub> brownmillerite. High Pressure Research, 2019, 39, 92-105.	1.2	4
47	Thermal expansion of ellinaite (β-CaCr2O4): an in-situ high temperature X-ray diffraction study. Physics and Chemistry of Minerals, 2021, 48, 1.	0.8	4
48	Phase transition of Mg3(PO4)2 polymorphs at high-temperature: In-situ synchrotron X-ray diffraction and Raman spectroscopic study. Spectrochimica Acta - Part A: Molecular and Biomolecular Spectroscopy, 2022, 269, 120762.	3.9	4
49	Raman spectroscopic and X-ray diffraction study of α- and β-Mg2P2O7 at various temperatures. Spectrochimica Acta - Part A: Molecular and Biomolecular Spectroscopy, 2022, 273, 121076.	3.9	3
50	Pressure- and temperature-dependent Raman spectra of Ca2Fe2O5 oxygen defect perovskite. Spectrochimica Acta - Part A: Molecular and Biomolecular Spectroscopy, 2022, 279, 121436.	3.9	3
51	X-ray diffraction studies of Sr3Cr2O8 and Ba3Cr2O8 at high pressures. Solid State Communications, 2014, 200, 5-8.	1.9	2
52	Pressure-dependent Raman spectra of Ba5(PO4)3Cl alforsite. Physics and Chemistry of Minerals, 2018, 45, 353-359.	0.8	2
53	X-ray diffraction and Raman spectra of merrillite at high pressures. High Pressure Research, 2020, 40, 411-422.	1.2	2
54	Thermal expansion and compressibility of calcium scandate CaSc2O4. Journal of Alloys and Compounds, 2022, 909, 164756.	5.5	2

SHUANGMENG ZHAI

#	Article	IF	CITATIONS
55	Equation of state of Ca2AlSiO5.5 oxygen defect perovskite. Physics and Chemistry of Minerals, 2015, 42, 327-336.	0.8	1
56	Electrical and thermal conductivity of Earth's core and its thermal evolution—A review. Acta Geochimica, 2022, 41, 665-688.	1.7	1
57	Crystal chemistry of Eu-bearing tuite synthesized at high-pressure and high-temperature conditions. Physics and Chemistry of Minerals, 2019, 46, 157-163.	0.8	Ο
58	Stability of low-pressure and high-pressure CaGa2O4 polymorphs at elevated temperatures: Raman spectroscopic study. Vibrational Spectroscopy, 2022, 120, 103379.	2.2	0